J IRAN CHEM SOC (2017) 14:791–801
DOI 10.1007/s13738-016-1029-1

ORIGINAL PAPER

Hollow Fe_3O_4@DA-SO_3H: an efficient and reusable heterogeneous nano-magnetic acid catalyst for synthesis of dihydropyridine and dioxodecahydroacridine derivatives

Marzie sadat Mirhosseyni[1] · Firouzeh Nemati[1] · Ali Elhampour[1]

Received: 4 August 2016 / Accepted: 5 December 2016 / Published online: 18 December 2016

Abstract In this work, for the first time, a highly stable and efficient super-paramagnetic catalyst, H-Fe_3O_4@DA-SO_3H, involving hollow morphology of Fe_3O_4 as core and dopamine as shell was prepared through hydrothermal template-free method. It has been used as a new and recoverable catalyst for various one-pot multi-component organic reactions such as synthesis of 1,4-dihydropyridine (1,4-DHP) and 1,8-dioxodecahyroacridine derivatives. The new magnetic catalyst was characterized with different analyses including X-ray powder diffraction (XRD), Fourier transform infrared spectroscopy (FT-IR), field emission scanning electron microscopy (FE-SEM), transmission electron microscopy (TEM), energy-dispersive X-ray spectroscopy (EDX), vibrating sample magnetometer (VSM) and thermogravimetric analysis (TGA). Moreover, the ρ_{shell} of the prepared hollow-Fe_3O_4 microparticles was calculated, being found just slightly lighter than that of solid sphere-like Fe_3O_4. The catalyst was conventionally recovered, using an external magnet and reused at least in six successive runs, without appreciable loss of its activity.

Graphical Abstract

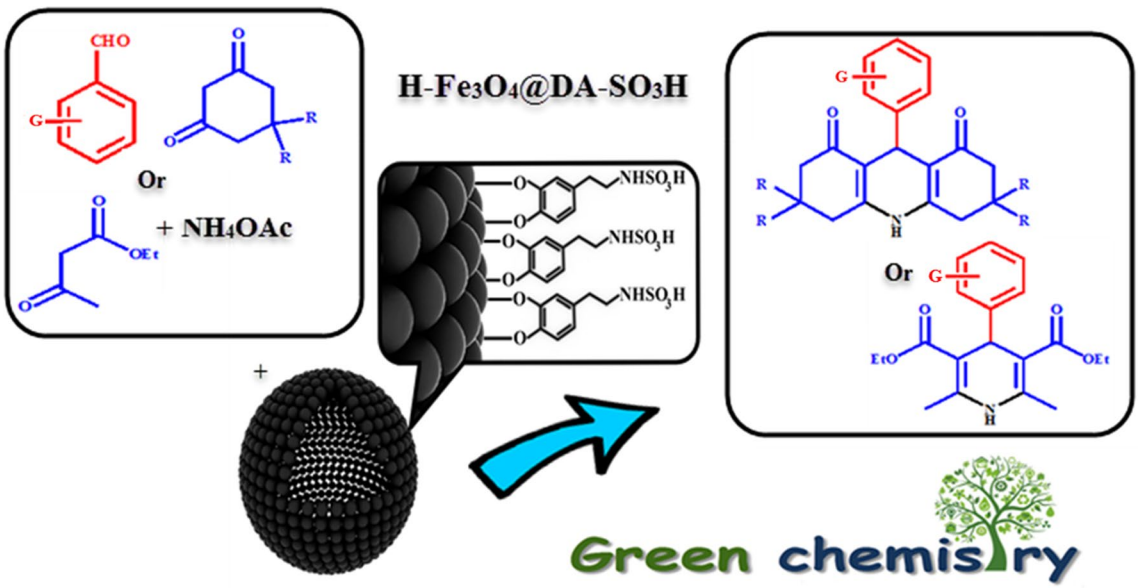

✉ Firouzeh Nemati
fnemati@semnan.ac.ir

[1] Department of Chemistry, Semnan University, 35131-19111 Semnan, Iran

Keywords Hollow magnetite · Green chemistry · Dopamine · Sulfamic acid · Multi-component organic reaction · Solvent free

Introduction

Hollow sphere particles (HSPs) have attracted much attention because of their special structure, physical and chemical properties such as well-defined morphology, uniform size, low density, light weight and high surface area which make them applicable in various fields such as drug delivery [1, 2], medicine [3], chemical sensors [4], fuel cells [5] and photonic materials [6]. In addition, many hollow-structure particles are used in various organic reactions as catalyst [7–17].

For these broad and prospective applications of HSPs, different methods have been developed to prepare these useful particles in different organic [18, 19] inorganic [20–22] and hybrid material types [23–25] including hard-template [26–28], soft-template [29, 30] and template-free [31–33] strategies.

On the other hand, the use of common Bronsted acidic catalysts such as HF, sulfuric or phosphoric acid bears various disadvantages such as high toxicity, waste generation and limited solubility phase contact with the starting materials. To overcome these drawbacks, homogenous acid catalysts were immobilized on the surface of magnetic solid-supported materials [34–38] which results in their simple separation by using an external magnet [39]. Among them, hollow-Fe_3O_4 particle has become an important object of research and attracts a growing interest because of its special physical and magnetic properties [40–43]. However, surface functionalization of hollow magnetic particles is an interesting way to fill the gap between homogenous and heterogeneous catalysts realm [44].

Dopamine (DA) is an important organic chemical of catecholamine families that plays several important roles in the brain and body and also is applicable in different branches of science such as pharmacy, biology and chemistry [45–47]. Recently, dopamine has been proposed as a novel organic coating material [48–57]. So another objective of this study was to investigate the role of dopamine as a linker of acidic functional group on the surface of hollow-Fe_3O_4 substrate.

In the present study, we chose dopamine (DA) as the linker to connect the $–SO_3H$ group to the iron oxide shell of the magnetic nanoparticles because the spectroscopic study by Rajh [58] suggested that bidentate enediol ligands such as DA convert the under-coordinated Fe surface sites back to a bulk-like lattice structure with an octahedral geometry for oxygen-coordinated iron, which may result in tight binding of DA to iron oxide. In continuation of our research work in the synthesis of new nano-magnetic catalysts [59–62] and their application in organic transformations [63–67], we are going to describe the first-time preparation and characterization of H-Fe_3O_4@DA-SO_3H magnetic nanoparticle as a superior heterogeneous acid (Scheme 1). This new synthesized catalyst has been successfully used for some one-pot multi-component reactions to synthesize different useful heterocyclic compounds such as 1,4-dihydropyridine (1,4-DHPs) and 1,8-dioxodecahydroacridine derivatives.

Experimental

Material and instrument

Chemical reagents in high purity were purchased from Merck and Aldrich and were used without further purification. Melting points were determined in open capillaries using an Electrothermal 9100 without further corrections. The progress of the reactions was monitored by TLC on commercial aluminum-backed plates of silica gel 60 F254, visualized, using ultraviolet light. X-ray diffraction (XRD) was detected by Philips using Cu-Ka radiation of wavelength 1.54Å. Scanning electron microscopy, FE-SEM–EDX, analysis was performed using Tescanvega II XMU digital scanning microscope. Samples were coated with gold at 10 mA for 2 min prior to analysis. The magnetic properties were characterized using a vibrating sample magnetometer (VSM, Lakeshore7407) at room temperature. The transmission electron microscopy (TEM) micrographs were taken with a CM30300Kv field emission transmission electron microscope. Thermogravimetric analyses (TGA) were conducted with a LINSEIS model STS PT 16000 thermal analyzer under air atmosphere at a heating rate of 5 °C min^{-1}. ^1H NMR and ^{13}C NMR spectra were recorded using a Bruker spectrometer at 500 and 125 MHz, respectively.

Preparation of catalyst

Preparation of H-Fe_3O_4

Firstly, the hollow-Fe_3O_4 particles were prepared according to literature report [68]. Following the procedure, first, $FeCl_3{\cdot}6H_2O$ (1.35 g, 5 mmol) and $NaOAc.3H_2O$ (3.85 g, 12.6 mmol) were dissolved in 25 ml ethylene glycol (EG), then 1 g PVP (polyvinylpyrrolidine) was dissolved in 15 ml EG and added to the first solution with a magnetic stirring for 15 min. The resulted solution was transferred to a 100-ml Teflon-lined stainless steel autoclave and heated at 200 °C for 12 h. The resulting black mixture was washed repeatedly with ethanol and deionized water (1:1). It was dried at 80 °C in an oven.

Scheme 1 Preparation of hollow Fe_3O_4@DA-SO_3H

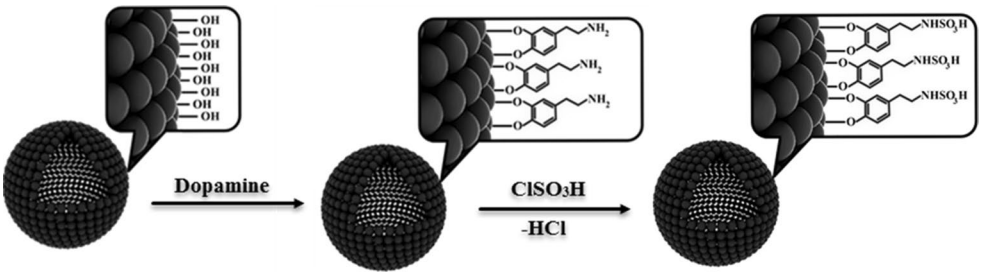

Preparation of H-Fe_3O_4@DA and H-Fe_3O_4@DA-SO_3H

To a stirred well suspension of H-Fe_3O_4 (1 g) in deionized water (50 ml) was dissolved dopamine (2 g) and refluxed for 12 h at 100 °C. The reaction mixture filtered using a magnet and filtrate (H-Fe_3O_4@DA) was washed with acetone and dried at 70 °C [54]. Then, in a flask, equipped with a constant-pressure dropping funnel and a gas inlet tube for conducting HCl gas over an adsorbing solution, H-Fe_3O_4@DA (1 g) was charged. Then, neat chlorosulfonic acid (0.3 ml, 4.5 mmol) was added drop-wise over a period of 15 min at room temperature. A voluminous evolution of HCl gas was observed. The mixture was stirred until HCl evolution ended up. Then, the H-Fe_3O_4@DA-SO_3H was collected as a black powder (0.9 g).

Loading of H^+

The loading of H^+ for the acidic magnetic nanoparticles was determined using potentiometric titration, and it was found to be 3.1 mmol/g.

General procedure for synthesis of 1,4-dihydropyridine (1,4-DHPs) and 1,8-dioxodecahydroacridine derivatives

The catalytic activity of H-Fe_3O_4@DA-SO_3H was also evaluated through condensation of various aldehyde (1) (1 mmol), ethyl acetoacetate (2) (2 mmol) or 1,3-cyclohexanedione (4) (2 mmol), NH_4OAc (2.5 mmol) and H-Fe_3O_4@DA-SO_3H (0.01 g) as catalyst at 100 °C under solvent-free condition. After completion of the reaction monitored by means of TLC (*n*-hexan: EtOAc 7:3), the reaction mixture diluted by hot EtOH and catalyst was separated from the mixture by means of an external magnet. The pure products were recrystallized from ethanol.

Spectroscopic data and physical properties of some selected compounds Diethy-l4-(4-chlorophenyl)-1,4-dihydro-2,6- dimethylpyridine-3,5- dicarboxylate (**3c**): light yellow solid; mp: 149 °C; IR ν_{max} (KBr): 827, 1118, 1622, 1650, 1475, 1212, 1688, 2958.60 and 3309.62 cm^{-1}; ^1H NMR (500 MHz, DMSO-D_6) δ: 8.84 (1H, s, N–H), 7.30–7.21 (2H, d, Ar–H), 7.20–7.16 (2H, d, Ar–H), 4.86 (1H, s, C–H), 3.95 (4H, q, CH_2), 2.27 (6H, s, 2Me) and 1.12 (6H, s, 2Me); ^{13}C NMR (125 MHz, DMSO-D_6) δ: 167.61, 147.98, 146.47, 131.28, 130.07, 128.63, 102.39, 59.89, 39.44, 19.06 and 14.98.

9-(4-chlorophenyl)-3,4,6,7-tetrahydro-3,3,6,6-tetramethylacridine 1,8(2H, 5H, 9H, 10H)-dione (**5c**): light yellow solid; mp: 297–299 °C; IR ν_{max} (KBr): 842, 1081.99, 1392.51, 1519.80,1691.46, 1714.60, 2956.67, 3103.25 and 3315.41 cm^{-1}; ^1H NMR (500 MHz, DMSO-D_6) δ: 9.32 (1H, s, N–H), 7.20 (2H, d, Ar–H), 7.16 (2H, d, Ar–H), 4.78 (1H, s, C–H), 2.49-1.97 (8H, m, $4CH_2$), 1.00 (6H, s, 2Me) and 0.85 (6H, s, 2Me); ^{13}C NMR (125 MHz, DMSO-D_6) δ: 195.2, 150.3, 146.9, 130.8, 130.3, 128.3, 111.9, 51.03, 33.54, 32.99, 29.90, 27.34.

Results and discussion

Preparation and characterization of hollow Fe_3O_4@DA-SO_3H

As shown in Scheme 1, in the first step, hollow-Fe_3O_4 nanoparticles were synthesized by hydrothermal treatment [68]. The next step involves the functionalization of hollow Fe_3O_4 with dopamine [54], and finally –SO_3H immobilized on the surface of H-Fe_3O_4@DA through covalent binding of sulfonic acid groups to the surface of a solid support using $ClSO_3H$ in an ice bath.

As shown in Fig. 1, the dopamine coordinated to the surface of the iron oxide nanoparticle because of the improved orbital overlap of the five-membered ring and a reduced steric repulsion around the iron complex [69].

FT-IR spectra

The FT-IR spectra of H-Fe_3O_4, H-Fe_3O_4@DA and H-Fe_3O_4@DA-SO_3H are depicted in Fig. 2. The Fe–O stretching vibration near 580 cm^{-1} was observed in all three spectra [70]. The significant features of H-Fe_3O_4@DA spectrum (Fig. 2b) are the appearance of the peaks about 3448, 3164, 1625 and 1400 cm^{-1}, which could be assigned to the –NH_2 and C–N stretching vibration of

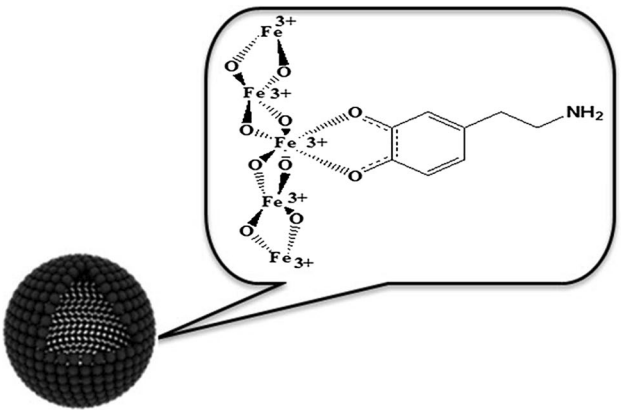

Fig. 1 Interaction of dopamine with H-Fe_3O_4

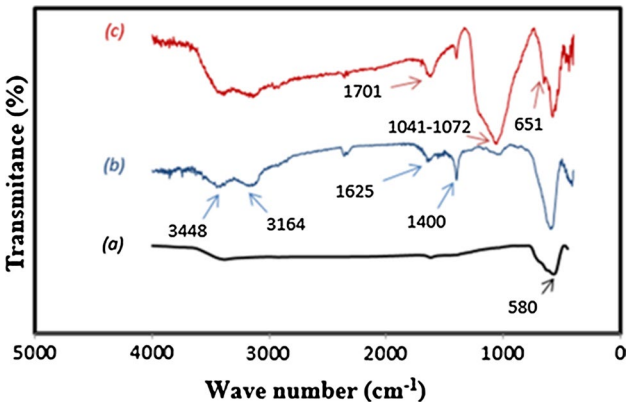

Fig. 2 FT-IR spectra of *a* H-Fe_3O_4, *b* H-Fe_3O_4@DA and *c* H-Fe_3O_4@DA-SO_3H

dopamine related to the surface of hollow MNPs [48]. In contrast, the grafting of acidic functional group (–SO_3H) in H-Fe_3O_4@DA-SO_3H was confirmed by weak S–O stretching vibration at 651 cm^{-1} and strong O=S symmetric stretching vibration about 1041–1072 cm^{-1} (Fig. 2c) [61]. The wide and strong absorbance peak at 2800–3400 cm^{-1} attributed to the –OH groups on the hollow MNPs' surface after modification and sulfonation (Fig. 2c). The increase in intensity of this band confirms that there are more –OH groups on the surface of final catalyst in comparison with the spectra of unmodified magnetic particles (a, b).

XRD spectra

The XRD analysis of H-Fe_3O_4, H-Fe_3O_4@DA, H-Fe_3O_4@DA-SO_3H was performed and the resulted comparative spectra are depicted in Fig. 3. The XRD spectrum of H-Fe_3O_4 shows the diffraction peaks at $2\theta = 30.06°$, 35.40°, 40.06°, 59.98°, 62.57° and 73.85° which can be assigned to the (220), (311), (400), (422), (511) and (440) planes of H-Fe_3O_4, respectively, that clearly matches with those of the literature report [71–73]. No other diffraction peaks were obtained, indicating high purity of the as-synthesized hollow-Fe_3O_4 products. However, the XRD pattern of H-Fe_3O_4@DA, H-Fe_3O_4@DA-SO_3H shows the broadband appearing in the range from 20° to 25° that is related to the presence of amorphous dopamine and dopamine –SO_3H shells formed around the magnetic hollow sphere that are not present in hollow-Fe_3O_4 species. As shown in Fig. 3b, c, there is not any considerable shift in the positions of the peaks, indicating the structural stability of H-Fe_3O_4 MNP during modification and sulfonation processes. Meanwhile, the average crystal size of H-Fe_3O_4 was also determined from X-ray pattern using Debye–Scherrer formula given as $\tau = K\,\lambda/\beta\,\mathrm{Cos}\,\theta$ is to be around 34.5 nm.

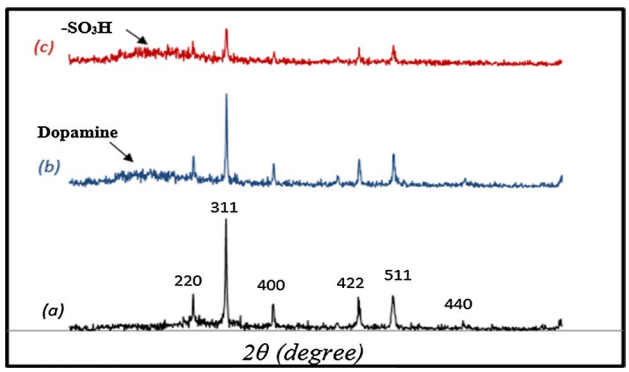

Fig. 3 XRD pattern of *a* H-Fe_3O_4, *b* H-Fe_3O_4@DA and *c* H-Fe_3O_4@DA-SO_3H

FE-SEM, EDX and TEM analyses

The size and morphology of H-Fe_3O_4 MNPs before and after the functionalization process were examined by means of SEM and TEM analyses. Figure 4 shows a typical SEM image of H-Fe_3O_4, H-Fe_3O_4@DA and H-Fe_3O_4@DA-SO_3H, respectively, that shows the particles are spherical in shape and nearly monodisperse in size. The elemental composition of H-Fe_3O_4, H-Fe_3O_4@DA and H-Fe_3O_4@DA-SO_3H was also determined from EDX spectra, which further confirmed the hollow Fe_3O_4 (Fig. 4d) modified with dopamine (Fig. 4e) and functionalized with –SO_3H (Figs. 4f, 5b–g). The presence of Au element is arising from the coating of materials by layer of Au in FE-SEM and EDX analyses.

The hollow structure was confirmed by TEM as shown in Fig. 5. In addition, a strong contrast between the dark edges and the pale center confirms the creation of hollow structures. The average diameter of core/shell

particles is around 500 nm, which is in agreement with SEM (Fig. 4c), indicating that the dopamine sulfonic acid shell covered hollow particles completely. As shown in Fig. 5, the sphere morphology is well preserved after modification.

TGA analysis

Thermal gravimetric analysis (TGA) of H-Fe_3O_4, H-Fe_3O_4@DA and H-Fe_3O_4@DA-SO_3H was used to confirm the successful preparation and thermal stability of catalyst as outlined in Fig. 6. The TGA curves present different mass loss range. In all three curves, a weight loss (about 10%) in the temperature range from 35 to 150 °C is attributed to the removal of the surface adsorbed water. In Fig. 6b, the weight loss (about 20%) up to 250 °C is related to removal of organic groups on the surface. The TGA curve for the H-Fe_3O_4@DA-SO_3H exhibits three-weight loss steps, which are assigned to the loss of water, decomposition of sulfamic acid and loss of organic groups. Based on these results, the successful grafting of dopamine sulfamic acid onto the surface of hollow Fe_3O_4 is verified.

Magnetization study

The magnetic properties of H-Fe_3O_4, H-Fe_3O_4@DA and H-Fe_3O_4@DA-SO_3H were studied by vibrating sample magnetometer (VSM) at room temperature and are presented in Fig. 7. The curves show no remnant magnetization or coercivity, indicating three samples are super-paramagnetic at room temperature. In addition, H-Fe_3O_4 shows relative high-saturation magnetization. So, H-Fe_3O_4 has super-paramagnetic behavior and high saturation magnetization properties, simultaneously [72, 74]. Considering the curves a, b and c in the Fig. 6, it is found that the saturation magnetization values of H-Fe_3O_4, H-Fe_3O_4@DA and H-Fe_3O_4@DA-SO_3H are 70.66, 50.85 and 37.35 emu/g, respectively. The decrease in the saturation magnetization of H-Fe_3O_4@DA and H-Fe_3O_4@DA-SO_3H is attributed to the contribution of the non-magnetic materials. The results indicated that the obtained catalyst would respond fast under external magnet.

Calculation of H-Fe_3O_4 density

It is important to determine the physical property of shell in hollow sphere particles, because it is the most considerable factor, which directly affects functionality of the final catalyst. So, in this study the shell density was determined using specific surface area and shell thickness as reported earlier in the literature [75].

The ρ_{shell} was calculated with shell thickness of "*t*" (nm) (obtained from XRD), inner radius of "*r*" (nm) (obtained from BET) and specific surface area SA ($m^2\ g^{-1}$) (obtained from BJH) [63]. Therefore, the ρ_{shell} value was calculated as follow: 4.73 $g.cm^{-3}$.

$$S_A = \frac{4\pi\{(r+t)^2 + r^2\}}{(4/3)\pi\rho\text{shell}\{(r+t)^3 - r^3\}}$$

The magnetite's density is established at 5.18 $g.cm^{-3}$ [76, 77], so the as-synthesized hollow spheres have lower density than solid sphere-like Fe_3O_4. It can be important for potential applications in industrial fields.

The catalytic activity of H-Fe_3O_4@DA-SO_3H at different one-pot multi- component reactions

Having synthesized and characterized the H-Fe_3O_4@DA-SO_3H, its role as a heterogeneous magnetically acid catalyst was then evaluated in the course of the synthesis of 1,4-dihydropyridine (1,4-DHPs) and 1,8-dioxodecahydroacridine derivatives. In order to optimize reaction conditions, the reaction of benzaldehyde (1 mmol) with ethyl acetoacetate (2 mmol) or dimedone (2 mmol) in the presence of NH_4OAc (2.5 mmol) to afford the corresponding products (3a and 5a) was selected as the model reactions. In this regard, various reaction parameters such as solvent, temperature and the amount of catalyst should be considered (Scheme 2).

In addition, with respect to the green chemistry considerations, the model reactions were carried out in solvent-free condition, too (Table 1). As Table 1 shows, in the absence of the catalyst, a low yield of the products has been obtained (Table 1, entry 8).

A variety of aromatic aldehydes bearing electron-donating or electron-withdrawing groups (Table 2, entries 1–9), aliphatic aldehyde (Table 2, entry 10) and heteroaromatic aldehyde (Table 2, entry 11) smoothly reacted with ethylacetoacetate and ammonium acetate to give the corresponding 1,4-DHPs in good-to-high yields and short reaction times. We also tested aromatic aldehydes with substituent in different positions (Table 2, entries 6–8). To our delight, ortho- and meta- substituted aromatic aldehydes were also very reactive and gave high yields of corresponding products.

Encouraged by these results, the optimized condition was also attempted to the synthesis a variety of 1,8-dioxodecahydroacridine derivatives (Table 3). Therefore, the reaction of different aldehydes with ammonium acetate and dimedone or 1,3-cyclohexanedione resulted in the formation of the corresponding products. The reactions were clean and the products result in high yield (94–80%) in reaction times ranging from 25 to 55 min. This method is equally effective with aldehydes bearing electron-withdrawing (Table 3, entries 2–8, 14–16 and 18–19),

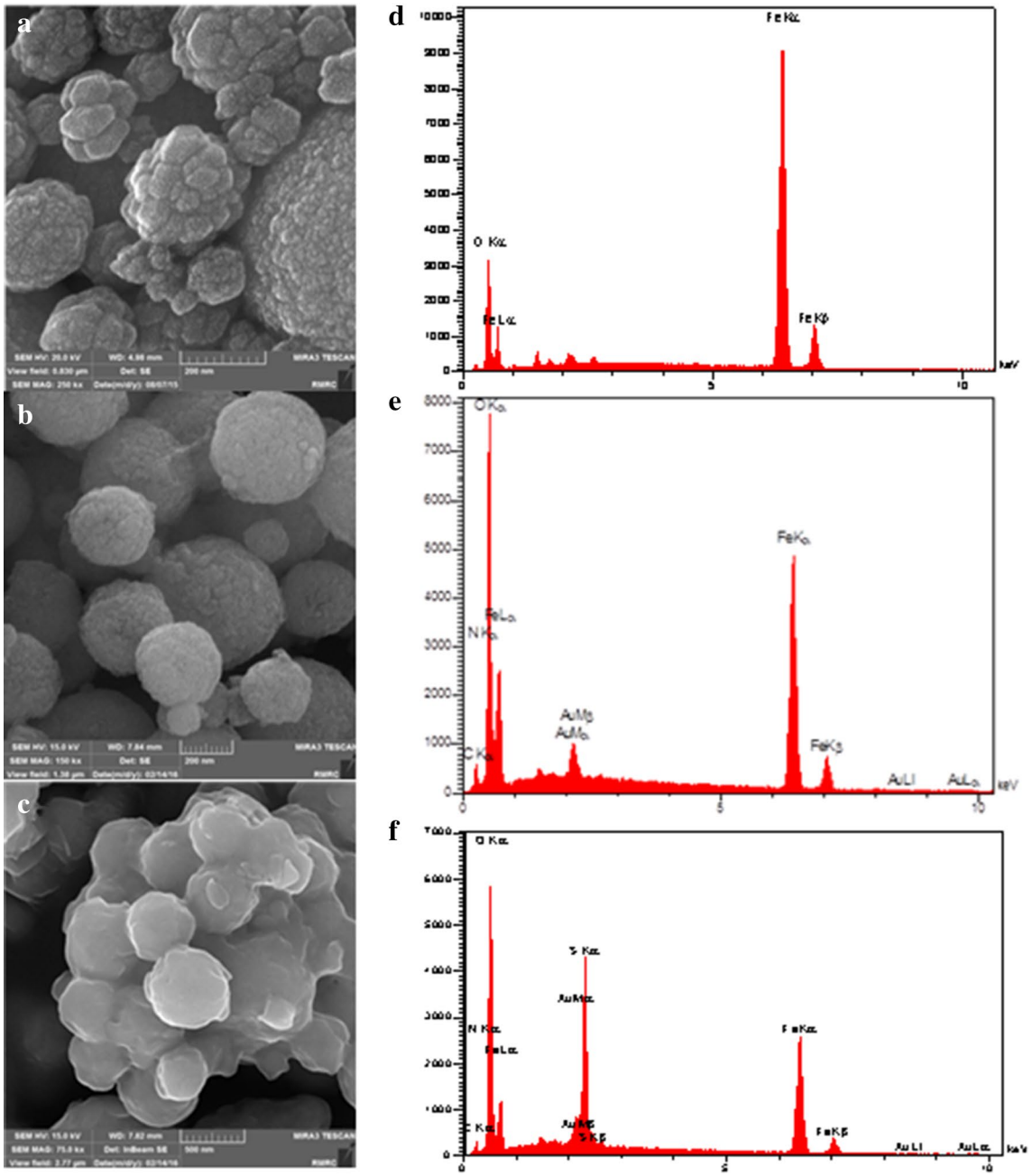

Fig. 4 FE-SEM–EDS analysis of H-Fe_3O_4 (**a**, **d**), H-Fe_3O_4@DA (**b**, **e**) and H-Fe_3O_4@DA-SO_3H (**c**, **f**)

electron-donating groups (Table 3, entries 9–11, 17 and 20) and aromatic rings containing bulky substituents (Table 3, entry 12).However, aliphatic aldehydes have no reaction activity in the novel method.

The comparison of the catalytic activity of H-Fe_3O_4@DA-SO_3H with various catalysts at different reaction conditions for synthesis of (3a) and (5a) compounds is listed in Table 4. The collected data clearly indicate that this new synthesized catalyst has many advantages in various fields such as reaction time, yield and catalytic activity.

Recyclability of catalyst

The reusability and recovery of the catalyst are important issues for the catalytic reactions, which make the method economically cheap, industrially profitable and environmentally sustainable. So, the reaction between benzaldehyde (1 mmol) and dimedone (2 mmol) under optimal reaction condition was selected to investigate the constancy of the catalyst activity for this model reaction. After completion of the reaction, hot ethanol was added to the reaction

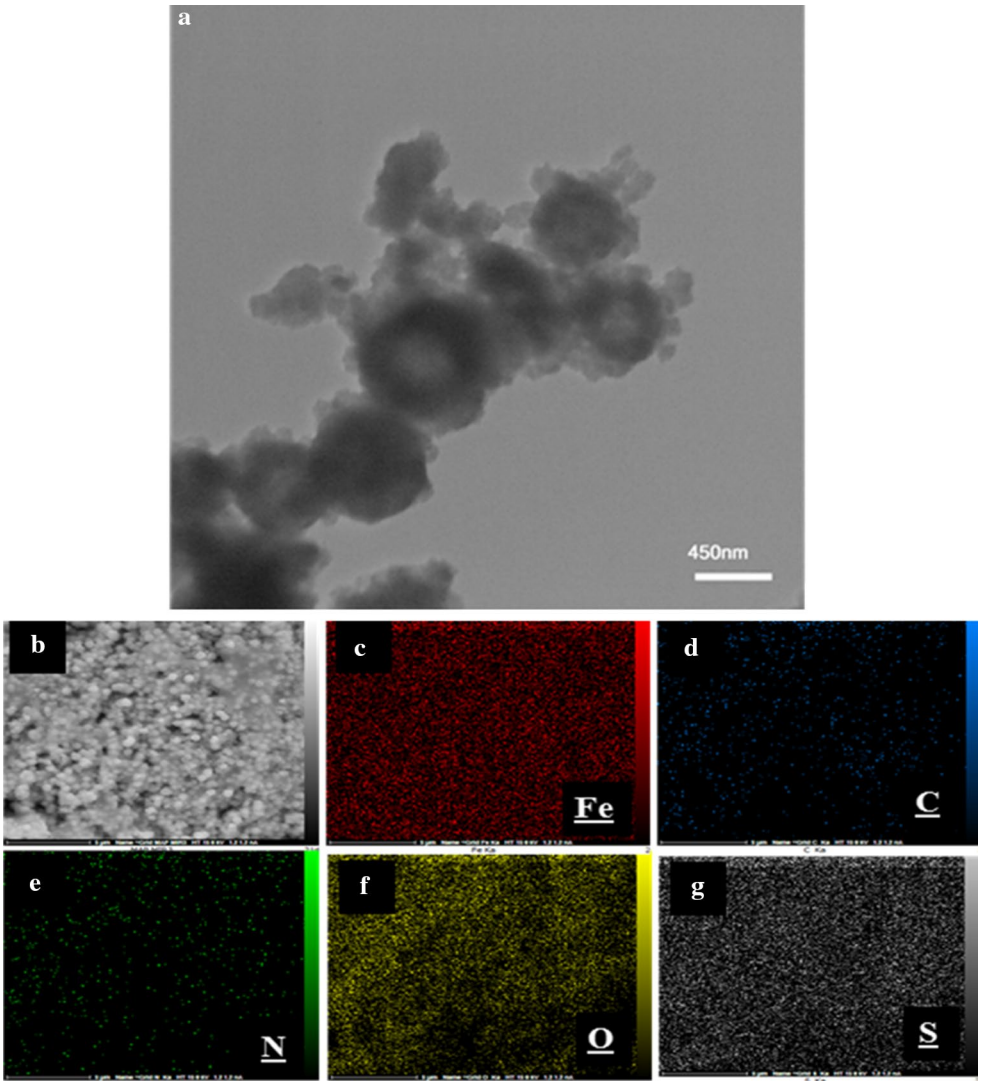

Fig. 5 TEM of H-Fe_3O_4@DA-SO_3H (**a**) and elemental mapping data of H-Fe_3O_4@DA-SO_3H (**b**–**g**)

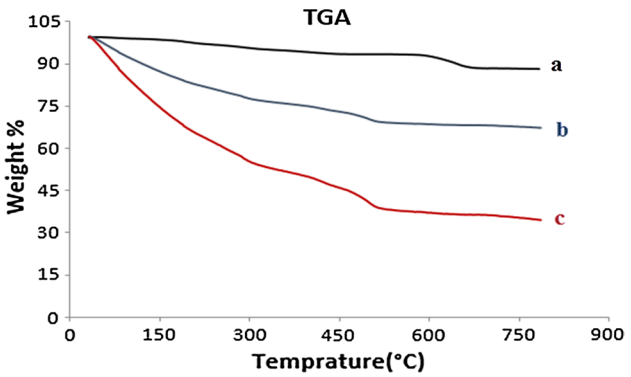

Fig. 6 TGA of *a* H-Fe_3O_4, *b* H-Fe_3O_4@DA and *c* H-Fe_3O_4@DA-SO_3H

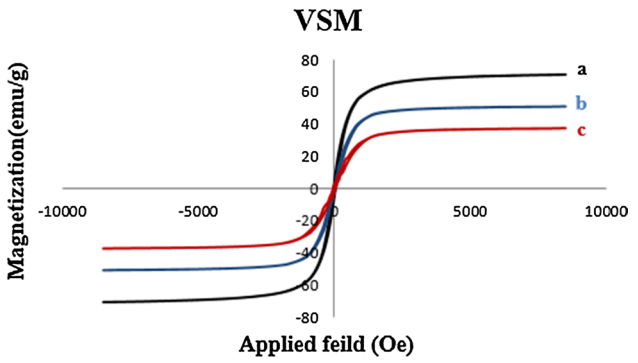

Fig. 7 Magnetization curves for H-Fe_3O_4 (*a*), H-Fe_3O_4@DA (*b*) and H-Fe_3O_4@DA-SO_3H (*c*)

mixture and the catalyst was easily separated using an external magnet. It was washed with ethanol, dried at 70 °C and used for the next cycle. The recovered catalyst could be added to fresh substrates of mentioned reaction for at least 6 times without any noticeable reduction in catalytic activity (Fig. 8).

Scheme 2 Model reactions for optimization of reaction condition for synthesis of **3a** and **5a**

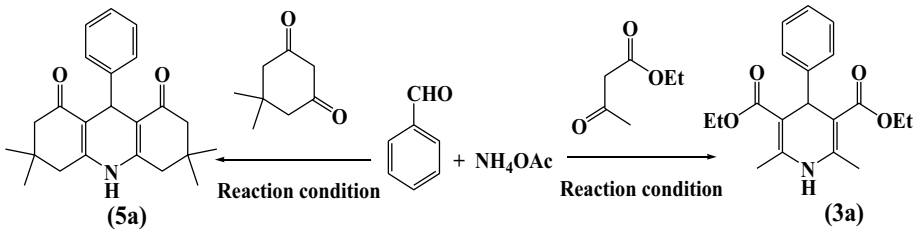

Table 1 Optimization of reaction condition for synthesis of 1,4-dihydropyridine and 1,8-dioxodecahydroacridine

No.	Catalyst (*g*)	Condition	Time (min)		Yield (%)[a]	
			8a	9a	8a	9a
1	0.005	Solvent free/80 °C	50	45	75	80
2	0.01	Solvent free/80 °C	45	40	75	80
3	0.005	Solvent free/90 °C	45	45	80	85
4	0.01	Solvent free/90 °C	40	40	80	85
5	0.01	Solvent free/100 °C	40	40	85	90
6	0.02	Solvent free/100 °C	40	40	85	90
7	0.04	Solvent free/100 °C	25	35	85	90
8	–	Solvent free/100 °C	60	60	Trace	
9	Fe_3O_4(0.01 g)	Solvent free/100 °C	40	40	54	55
10	Fe_3O_4@DA (0.01 g)	Solvent free/100 °C	40	40	32	45
11	DA (0.01 g)	Solvent free/100 °C	40	40	Trace	

Reaction condition: benzaldehyde (1 mmol), ethyl acetoacetate or dimedone (2 mmol), NH_4OAc (2.5 mmol)

[a] Isolated yield

Table 2 Synthesis of 1,4-dihydropyridine derivatives

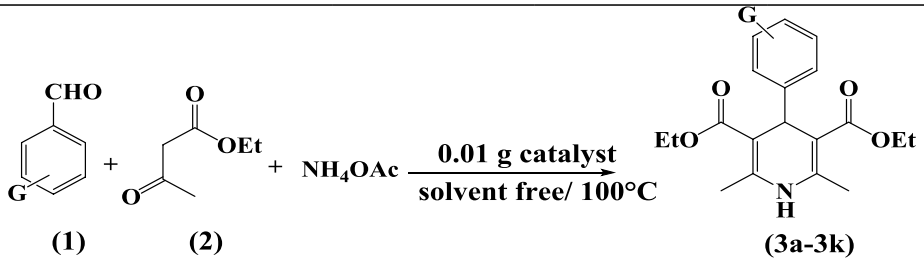

No.	Aldehyde	Product	Time (min)	Yield (%)[a]	M.P. (°C)
1	OHC–C_6H_5	3a	40	85	157–158 [78]
2	2-Cl–C_6H_4–CHO	3b	25	92	126–128 [79]
3	4-Cl–C_6H_4–CHO	3c	45	88	149 [80]
4	4-Br–C_6H_4–CHO	3d	30	85	165–167 [78]
5	4-F–C_6H_4–CHO	3e	25	84	147-148 [80]
6	2-O_2N–C_6H_4–CHO	3f	35	87	162–164 [81]
7	3-O_2N–C_6H_4–CHO	3 g	40	85	160–161 [82]
8	4-O_2N–C_6H_4–CHO	3 h	45	83	129–130 [78]
9	4-MeO–C_6H_4–CHO	3i	25	85	157–158 [80]
10	Cinnamaldehyde	3j	25	79	139–140 [80]
11	Thiophen-2-carbaldehyde	3 k	20	86	169–170 [82]

Reaction condition: aldehyde (1 mmol), ethyl acetoacetate (2 mmol), NH_4OAc (2.5 mmol), H-Fe_3O_4@DA-SO_3H (0.01 g), under solvent-free condition at 100 °C

[a] Isolated yield

Table 3 Synthesis of 1,8-dioxodecahydroacridine derivatives

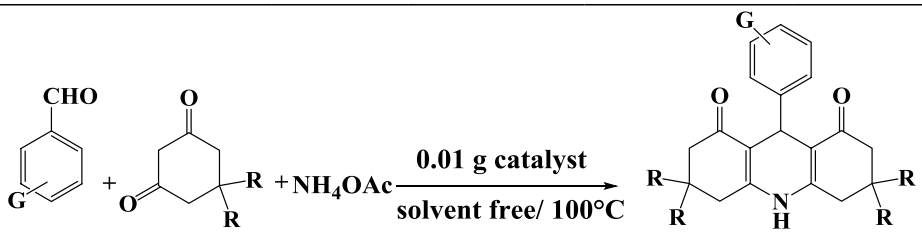

(1) (4) (5a-5l)and (6a-6h)

No.	Aldehyde	R_1	Product	Time (min)	Yield (%)[a]	M.P. (°C)
1	OHC–C_6H_5	Me	5a	40	90	290–291 [34]
2	2-Cl–C_6H_4–CHO	Me	5b	35	88	225–227 [34]
3	4-Cl–C_6H_4–CHO	Me	5c	40	92	297–299 [34]
4	4-Br–C_6H_4–CHO	Me	5d	35	90	312–313 [34]
5	4-F–C_6H_4–CHO	Me	5e	25	90	292–293 [34]
6	2-O_2N–C_6H_4–CHO	Me	5f	45	85	284–286 [34]
7	3-O_2N–C_6H_4–CHO	Me	5 g	45	90	282–284 [34]
8	4-O_2N–C_6H_4–CHO	Me	5 h	40	94	302–303 [34]
9	4-$(CH_3)_2N$–C_6H_4–CHO	Me	5i	30	85	265–267 [34]
10	4-Me–C_6H_4–CHO	Me	5j	40	90	268–270 [34]
11	4-MeO–C_6H_4–CHO	Me	5 k	40	90	269–271 [34]
12	2-Naphtaldehyde	Me	5 l	40	85	264–266 [34]
13	OHC–C_6H_5	H	6a	50	89	279–280 [34]
14	2-O_2N–C_6H_4–CHO	H	6b	45	85	295–298 [83]
15	3-O_2N–C_6H_4–CHO	H	6c	35	90	280–281 [34]
16	4-O_2N–C_6H_4–CHO	H	6d	35	92	295–296 [83]
17	4-Me–C_6H_4–CHO	H	6e	35	92	253–254 [34]
18	4-Cl–C_6H_4–CHO	H	6f	40	90	295–296 [34]
19	4-Br–C_6H_4–CHO	H	6 g	40	85	310–311 [34]
20	4-MeO–C_6H_4–CHO	H	6 h	55	80	302–304 [34]

Reaction condition: aldehyde (1 mmol), dimedone or 1,3-cyclohexanedione (2 mmol), NH_4OAc (2.5 mmol), H-Fe_3O_4@DA-SO_3H (0.01 g), under solvent-free condition at 100 °C

[a] Isolated yield

Table 4 Comparison of the catalytic activity of H-Fe_3O_4@DA-SO_3H with various catalysts

No.	Catalyst	Condition	Product	Time (min)	Yield (%)
1	TiO_2 NPs	EtOH/reflux	3a	135	92 [78]
2	Fe-TDU-1	EtOH/80 °C	3a	300	76 [84]
3	*n*-FTSA[a]	Solvent free/110 °C	5a	50	95 [85]
4	*n*-ZrSA[b]	Solvent free/100 °C	5a	45	91 [34]
5	Benzyltrimethylammoniumfluoride hydrate	Solvent free/70 °C	3i	15	89 [86]
6	Chitosan	Solvent free/80 °C	3a	20	90 [87]
7	Dimethyl phosphate ionic liquids	Solvent free/80 °C	3a	180	61 [88]
8	Vanadatesulfuric acid	Solvent free/80 °C	5a	20	93 [89]
9	Fe_3O_4 (0.024 g)	Solvent free/80 °C	5a	5	92 [39]
10	H-Fe_3O_4@DA-SO_3H (0.01 g)	Solvent free/100 °C	3a	40	85[c]
11	H-Fe_3O_4@DA-SO_3H (0.01 g)	Solvent free/100 °C	5a	40	90[c]

[a] Nano-Fe_3O_4–TiO_2–SO_3H

[b] Nano-ZrO_2–SO_3H

[c] This work

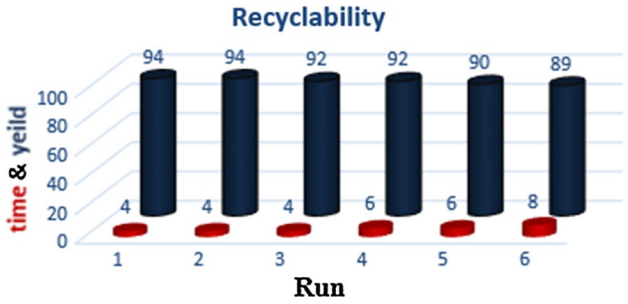

Fig. 8 Catalyst recyclability experiment

Conclusions

In summary, the new hollow-Fe_3O_4-supported dopamine sulfamic acid was introduced as an efficient and low-density catalyst for different multi-component organic reactions including synthesis of 1,4-dihydropyridine and 1,8-dioxodecahydroacridine derivatives under solvent-free condition. The novel catalyst could be recovered in a facile manner from the reaction mixture and a good yield was observed even after the catalyst was recycled six times.

Acknowledgements The authors gratefully acknowledge Semnan University Research Council for financial support of this work.

References

1. J. Shin, R.M. Anisur, M.K. Ko, G.H. Im, J.H. Lee, I.S. Lee, Angew. Chem. Int. Ed. **48**, 321 (2009)
2. J.F. Chen, H.M. Ding, J.X. Wang, L. Shao, Biomaterials **25**, 723 (2004)
3. J. Gao, J. Chen, X. Li, M. Wang, X. Zhang, F. Tan, S. Xu, J. Liu, J. Colloid Interface Sci. **444**, 38 (2015)
4. S. Ameen, M.S. Akhtar, H.K. Seoa, H. Shina, Chem. Eng. J. **270**, 564 (2015)
5. X. Lai, J.E. Halpert, D. Wang, Energy Environ. Sci. **5**, 5604 (2012)
6. G. Duan, W. Cai, Y. Luo, F. Sun, Adv. Funct. Mater. **17**, 644 (2007)
7. P. Wang, H. Zhu, M. Liu, J. Niu, B. Yuan, R. Li, J. Ma, RSC Adv. **4**, 28922 (2014)
8. J. Niu, M. Liu, P. Wang, Y. Long, M. Xie, R. Li, J. Ma, N. J. Chem. **38**, 1471 (2014)
9. H. Kang, H. Lee, J. Park, H. Song, K. Park, Top. Catal. **53**, 523 (2010)
10. F. Zhang, Y. Wei, X. Wu, H. Jiang, W. Wang, H. Li, J. Am. Chem. Soc. **136**, 13963 (2014)
11. X. Wu, L. Tan, D. Chen, X. Meng, F. Tang, Chem. Commun. **50**, 539 (2014)
12. H. Li, Z. Zhu, J. Liu, S. Xie, H. Li, J. Mater. Chem. **20**, 4366 (2010)
13. Y. Guo, Y.T. Xu, G.H. Gao, T. Wang, B. Zhao, X.Z. Fu, R. Sun, C.P. Wong, Catal. Commun. **58**, 40 (2015)
14. C.C. Nguyen, N.N. Vu, T.O. Do, J. Mater. Chem. A **4**, 4413 (2016)
15. M. Sasidharan, S. Anandhakumar, P. Bhanja, A. Bhaumik, J. Mol. Catal. A: Chem. **411**, 87 (2016)
16. C. Deng, X. Ge, H. Hu, L. Yao, C. Han, D. Zhao, Cryst. Eng. Comm. **16**, 2738 (2014)
17. J.Y. Kim, J.C. Park, H. Kang, H. Song, K.H. Park, Chem. Commun. **46**, 439 (2010)
18. J. Chattopadhyay, T.S. Pathak, R. Srivastava, A.C. Singh, Electrochim. Acta **167**, 429 (2015)
19. H. Lv, G. Ji, W. Liu, H. Zhanga, Y. Dub, J. Mater. Chem. C. **3**, 10232 (2015)
20. Y. Yang, W. Zhang, Y. Zhang, A. Zheng, H. Sun, X. Li, S. Liu, P. Zhang, X. Zhang, Nano Res. **8**, 3404 (2015)
21. M. Chen, L. Wu, S. Zhou, B. You, Adv. Mater. **18**, 801 (2006)
22. C. Zhou, K. Huang, L. Yuan, W. Feng, X. Chu, Z. Geng, X. Wu, L. Wang, S. Feng, N. J. Chem. **39**, 2413 (2015)
23. Z. Teng, X. Su, Y. Zheng, J. Zhang, Y. Liu, S. Wang, J. Wu, G. Chen, J. Wang, D. Zhao, G. Lu, J. Am. Chem. Soc. **137**, 7935 (2015)
24. M.K. Kim, D.W. Kim, D.W. Shin, S.J. Seo, H.K. Chung, J.B. Yoo, Phys. Chem. Chem. Phys. **17**, 2416 (2015)
25. M. Ohnishi, Y. Kozuka, Q.L. Ye, H. Yoshikawa, K. Awaga, R. Matsuno, M. Kobayashi, A. Takahara, T. Yokoyama, S. Bandow, S. Iijima, J. Mater. Chem. **16**, 3215 (2006)
26. M. Chen, L. Wu, S. Zhou, B. You, Adv. Mater. **18**, 801 (2006)
27. M.M. Titirici, M. Antonietti, A. Thomas, Chem. Mater. **18**, 3808 (2006)
28. M. Shokouhimehr, J.E. Lee, S.I. Hana, T. Hyeon, Chem. Commun. **49**, 4779 (2013)
29. Z. Wang, M. Chen, L. Wu, Chem. Mater. **20**, 3251 (2008)
30. Y. Zhao, J. Zhang, W. Li, C. Zhang, B. Han, Chem. Commun. **2365** (2009)
31. B. Liu, H.C. Zeng, Small **1**, 566 (2005)
32. J. Li, H.C. Zeng, J. Am. Chem. Soc. **129**, 15839 (2007)
33. Z. Wang, L. Wu, M. Chen, S. Zhou, J. Am. Chem. Soc. **131**, 11276 (2009)
34. A. Amoozadeh, S. Rahmani, B. Bitaraf, F. Bolghan Abadi, E. Tabrizian, N. J. Chem. **40**, 770 (2016)
35. N. Koukabi, E. Kolvari, M.A. Zolfigol, A. Khazaei, B. Saghasemi, B. Fasahati, Adv. Synth. Catal. **354**, 2001 (2012)
36. E. Kolvari, N. Koukabi, M.M. Hosseini, M. Vahidian, E. Ghobadi, RSC Adv. **6**, 7419 (2016)
37. M. A. Zolfigol, M. Yarie, Appl. Organometal. Chem. (2016). doi:10.1002/aoc.3598
38. K. Debnath, K. Singha, A. Pramanik, RSC Adv. **5**, 31866 (2015)
39. M. Nasr-Esfahani, S.J. Hoseini, M. Montazerozohori, R. Mehrabi, H. Nasrabadi, J. Mol. Catal. A: Chem. **382**, 99 (2014)
40. T. Yao, H. Wang, Q. Zuo, J. Wu, B. Xin, F. Cui, T. Cui, J. Colloid Interface Sci. **450**, 366 (2015)
41. P. Wang, H. Zhu, M. Liu, J. Niu, B. Yuan, R. Li, J. Ma, RSC Adv. **4**, 28922 (2014)
42. S. Xuan, W. Jiang, X. Gong, Y. Hu, Z. Chen, J. Phys. Chem. C **113**, 553 (2009)
43. H. Liu, P. Wang, H. Yang, J. Niu, J. Ma, N. J. Chem. **39**, 4343 (2015)
44. M.B. Gawande, P.S. Brancoa, R.S. Varma, Chem. Soc. Rev. **42**, 3371 (2013)
45. H. Peng, X. Zhang, K. Huang, H. Xu, J. Wuhan. Univ. Technol. Mat. Sci. Ed. **23**, 480 (2008)
46. B. Mirzayi, A. Nematollahzadeh, S. Seraj, Powder Technol. **270**, 185 (2015)
47. M. Martın, P. Salazar, R. Villalonga, S. Campuzano, J.M. Pingarron, J. Gonzalez-Mora, J. Mater. Chem. B **2**, 739 (2014)
48. V. Polshettiwar, B. Baruwati, R.S. Varma, Green Chem. **11**, 127 (2009)
49. V. Polshettiwar, M.N. Nadagouda, R.S. Varma, Chem. Commun. **6318** (2008)

50. B.R. Vaddula, A. Saha, J. Leazer, R.S. Varma, Green Chem. **14**, 2133 (2012)
51. A. Saha, J. Leazer, R.S. Varma, Green Chem. **14**, 67 (2012)
52. D. Losic, Y. Yu, M.S. Aw, S. Simovic, B. Thierry, J. Addai-Mensah, Chem. Commun. **46**, 6323 (2010)
53. R.B. Nasir Baig, R.S. Varma, Chem. Commun. **48**, 2582 (2012)
54. D. Guin, B. Baruwati, S.V. Manorama, Org. Lett. **9**, 1419 (2007)
55. O. Gleeson, R. Tekoriute, Y.K. Gun,ko, S.J. Connon, Chem. Eur. J. **15**, 5669 (2009)
56. M. Hajjami, A. Ghorbani-Choghamarani, R. Ghafouri-Nejad, B. Tahmasbi, N. J. Chem. **40**, 3066 (2016)
57. Ch. Lei, F. Han, D. Li, W.-C. Li, Q. Sun, X.-Q. Zhang, A.-H. Lu, Nanoscale. **5**, 1168 (2013)
58. L.X. Chen, T. Liu, M.C. Thurnauer, R. Csencsits, T. Rajh, J. Phys. Chem. B **106**, 8539 (2002)
59. F. Nemati, M.M. Heravi, A. Elhampour, RSC Adv. **5**, 45775 (2015)
60. F. Nemati, A. Elhampour, H. Farrokhi, M.B. Natanzi, Catal. Commun. **66**, 15 (2015)
61. F. Nemati, S. Sabaqian, J. Saudi Chem. Soc. (2014). doi:10.1016/j.jscs.2014.04.009
62. F. Nemati, M.M. Heravi, R. Saeedirad, Chin. J. Catal. **33**, 1825 (2012)
63. A. Elhampour, M. Malmir, E. Kowsari, F. Boorboor ajdarib, F. Nemati, RSC Adv. **6**, 96623 (2016)
64. F. Nemati, R. Saeedirad, Chin. Chem. Lett. **24**, 370 (2013)
65. F. Nemati, A. Elhampour, S. Zulfaghari, Phosphorus, Sulfur Silicon Relat. Elem. **190**, 692 (2015)
66. F. Nemati, A. Elhampour, M.B. Natanzi, S. Sabaqian, J. Iran. Chem. Soc. **13**, 1045 (2016)
67. F. Nemati, A. Elhampour, Sci. Iranica C **19**, 1594 (2012)
68. Q.Q. Xiong, J.P. Tu, Y. Lu, J. Chen, Y.X. Yu, Y.Q. Qiao, X.L. Wang, C.D. Gu, J. Phys. Chem. C **116**, 6495 (2012)
69. M.D. Shultz, J.U. Reveles, S.N. Khanna, E.E. Carpenter, J. Am. Chem. Soc. **129**, 2482 (2007)
70. S.P. Pawar, D.A. Marathe, K. Pattabhi, S. Bose, J. Mater. Chem. A **3**, 656 (2015)
71. J. Niu, M. Xie, X. Zhu, Y. Long, P. Wang, R. Li, J. Mol. Catal. A: Chem. **392**, 247 (2014)
72. A. Naghipour, A. Fakhri, Catal. Commun. **73**, 39 (2016)
73. J. Safari, Z. Zarnegar, J. Mol. Catal. A: Chem. **379**, 269 (2013)
74. W. Cheng, K. Tang, Y. Qi, J. Sheng, Z. Liu, J. Mater. Chem. **20**, 1799 (2010)
75. C. Takai, H. Watanabe, T. Asai, M. Fuji, Colloids. Surf. A: Physicochem. Eng. Aspects **404**, 101 (2012)
76. Z.R. Marand, M.H.R. Farimani, N. Shahtahmasebi, Nanomed. J. **1**, 238 (2014)
77. L. Blaney, Lehigh Univ. **15**, 33 (2007)
78. M. Tajbakhsh, E. Allaee, H. Alinezhad, M. Khanian, F. Jahani, S. Khaksar, P. Rezaee, M. Tajbakhsh, Chin. J. Catal. **33**, 1517 (2012)
79. Y.L.N. Murthy, A. Rajack, M.T. Ramji, J.J. Babu, C. Praveen, K.A. Lakshmi, Bioorg. Med. Chem. Lett. **22**, 6016 (2012)
80. E. Priede, A. Zicmanis, Helvetica Chim. Acta **98**, 1095 (2015)
81. S. Wang, Z. Li, J. Zhang, J. Li, Ultrason. Sonochem. **15**, 677 (2008)
82. J. Safari, F. Azizi, M. Sadeghi, N. J. Chem. **39**, 1905 (2015)
83. M. Nasr-Esfahani, M. Montazerozohori, T. Abdizadeh, C. R. Chimie. **18**, 547 (2015)
84. V.V. Srinivasan, M.P. Pachamuthu, R. Maheswari, J. Porous Mater. **22**, 1187 (2015)
85. A. Amoozadeh, S. Golian, S. Rahmani, RSC Adv. **5**, 45974 (2015)
86. A. Khaskel, P. Barman, Heteroat. Chem. **27**, 114 (2016)
87. J. Safari, F. Azizi, M. Sadeghi, New J. Chem. **39**, 1905 (2015)
88. E. Priede, A. Zicmanis, Helv. Chim. Acta **98**, 1095 (2015)
89. M. Nasr-Esfahani, M. Montazerozohori, T. Abdizadeh, C. R. Chimie **18**, 547 (2015)